Computational and experimental studies on SnO_2 thin films at various temperatures

K. Gurushankar [1,2], M. Grishina [1], M. Gohulkumar [3], K. Kannan [4]
[1] Laboratory of Computational Modeling of Drugs, Higher Medical and Biological School, 454080, Russia, Chelyabinsk, South Ural State University;
[2] Department of Physics, Kalasalingam Academy of Research and Education, 626126, Krishnankoil, Tamilnadu, India;
[3] Vivekanandha College of Arts and Science for Women, Tiruchengode, Tamil Nadu, India;
[4] School of Advanced Materials Science and Engineering, Kumoh National Institute of Technology, 61 Daehak-ro, Gumi-si, Gyeongbuk, Republic of Korea

Abstract

Tin oxide (SnO_2) thin films was prepared by dip-coating technique at various bath temperatures (313, 333, 353 and 373 K) and annealed at 673 K in this study. And the obtained results were studied and correlated with the computational method. Scanning electron microscopy (SEM) investigation demonstrated that the prepared samples are spherical with agglomeration. The elemental analysis (EDAX) confirms the presence of Sn and O. Further, the SnO_2 thin films microstructures are simulated, their thermodynamic and surface properties have been calculated. Micro-Raman spectra were recorded for the prepared samples. Micro-Raman results exhibit the first-order Raman mode E_{1g} (475 cm^{-1}) indicating that the grown SnO_2 belongs to the rutile structure. In addition, the envelope method used for studying optical characteristics of the thin films from the transmittance spectra. The semiconducting nature of the films has been noticed from linear I-V characteristics. Furthermore, the electrical conductivity studies suggest that the highest conductivity samples acquire the lowest activation energy and their values are also in the semiconducting range.

Keywords: SnO_2 thin films, dip-coating technique, computational method, thermodynamic and surface characteristics, gibbs free energy and electrical conductivity.

Citation: Gurushankar K, Grishina M, Gohulkumar M, Kannan K. Computational and experimental studies on SnO_2 thin films at various temperatures. Computer Optics 2023; 47 (1): 53-61. DOI: 10.18287/2412-6179-CO-1151.

Introduction

Electrically conducting highly transparent thin films has aroused curiosity among the scientific community to discover new innovative materials with desirable properties, makes them find potential applications in the fields of optoelectronic devices, solar cells, and hybrid microelectronics [1 – 3]. Transparent conducting oxides (TCO) are excellent semiconductors which display a high transmission in the visible region and also it has high electrical conductivity. Among the different TCOs, Tin oxide (SnO_2), the most stable oxide of tin, is a metal oxide semiconductor that finds its use in a number of applications in the field of display devices, solar cells, light-emitting diodes, laser diodes, and solid-state gas sensors due to its interesting wide band gap, and its excellent thermal, mechanical and chemical stability [4, 5]. SnO_2 is an n-type wide bandgap semiconductor oxide with a high direct bandgap (Eg) in the 3.6 – 3.9 eV range at room temperature, making it extremely transparent in the visible region [6, 7]. Several techniques, including magnetron sputtering [8], chemical vapor deposition [9], atomic layer deposition [10], pulsed laser deposition [11], spray pyrolysis [12], and sol-gel [13], can be used to develop SnO_2 that is either undoped or doped. Among the various preparative methods, the sol-gel dip-coating technique has proved to be the most well-known method for fabricating thin films at nanoscale. Even though the preparation of thin films by this technique is being simple and low cost, the main advantage of it is the ability to form inorganic structures at relatively low temperatures. SEM with EDAX, UV-Vis, and electrical analysis used to classify SnO_2 thin films prepared by dip-coating method at various temperatures (313, 333, 353 and 373 K) and annealed at 673 K using $SnCl_2$ as a precursor. Further, correlated and discussed the results obtained from the experiment with computational method.

Materials and methods

Due to enhance good structural qualities, easy to produce coatings, and high purity materials at a low cost on a variety of substances dip-coating method is more appropriate for the preparation of films [14]. In the current study, dip coating method has used to prepare SnO_2 thin films and described briefly in our previously published research protocol [15]. In general, $SnCl_2$ or $SnCl_4$ has used as precursors. In the present study, anhydrous $SnCl_2$ has used as a precursor to prepare SnO_2 thin film [16, 17].

Pure SnO_2 sols were prepared at 1:9:9:6 molar ratio of anhydrous $SnCl_2$, distilled water, n-propanol [C_3H_7OH], and i-proponal [2-C_3H_7OH], respectively [14, 16, 17]. Initially, the precursor was dissolved into 66.3 % of the total

amount n-propanol. In addition, prehydrolysis of the $SnCl_2$, we add 33 % of the distilled water total amount suspended in remaining n-propanol (C_3H_7OH). For one hour it was stirred continuously and then earlier prepared sol was mixed with the solution of the remaining amount of water dissolve in the known amount of 2-C_3H_7OH. It was again stirred for one hour in a continuous manner for obtaining clear and homogenous sols. Finally, SnO_2 thin film was formed. Further, the bath temperature changed from 313-373 K in a step of 20 K, and then the films were annealed at 673 K.

X-ray diffraction characterization study of sample analysis described in previously [15]. The morphological studies of SnO_2 thin films were investigated by SEM (JSM 6390 JEOL) and the elemental composition was analyzed by EDAX. UV-Vis-NIR spectrophotometer (Perkin-Elmer Lambda 35) is used for recording the optical absorption spectrum. Electrical studies were carried out using a Keithley electrometer 6517 B.

Calculation of the thermodynamic and surface characteristics of SnO_2 thin films at all temperatures was carried out using MERA software with periodic boundary conditions along a and b axes of SnO_2 unit cell like it was described in [18,19] and applied in studying organic, inorganic and combined systems in [18 – 36]. The MOPS algorithm has also shown previous successful use in modeling oxyhydrate gel formation [18 – 36], crystal structures of triosmium clusters [20, 21], complexation of organic molecules during chemical reactions [22, 24, 28, 33, 35], and crystal structures and interaction energies of gas hydrates [18, 19]. The measured energies, thermodynamic characteristics (such as enthalpies, entropies, and Gibbs free energies), modeled structures of the complexes, crystals, and clusters, predicted yields, rates, and regio- and stereo-specificity of the reactions, and predicted yields, rates, and regio- and stereo-specificity of the reactions were all in good agreement with experimental results previously stated in the publications mentioned above.

Results and discussion

XRD studies of the deposited thin films established tetragonal rutile crystalline structure and the detected diffraction peaks 33.41°, 26.4°, 23.6°, 23, 17.6°, 16.7° and 15.9°, and it is very well matching h k l planes (1 1 0), (1 0 1), (2 0 0), (1 1 1), (2 1 1), (2 2 0) and (2 0 0), respectively. The low intensity peak in the XRD pattern of the dip coated tin oxide thin film prepared at bath temperatures of 313 K and 333 K suggests that these films are almost entirely non-crystalline and giving the information about that the material is amorphous. On the other hand, the films prepared at 353 K and 373 K have increased intensity, as well as additional peaks also observed and listed in detail in previous study [15]. Along with results, tin oxide films deposited (353 K and 373 K) have shown to be crystalline. It has been observed that as the bath temperature rises, the crystalline nature also rises, as previously mentioned [15]. The surface morphology of SnO_2 thin films was investigated by JEOL JSM-6390 LV SEM and it is one of the best tools for investigating surface smoothness and grain size of particle finding. The surface morphology of SnO_2 thin films prepared at different bath temperatures of 313, 333, 353 and 373 K shown in fig. 1. The SnO_2 thin films are in a spherical shape with agglomeration [37]. The film has cracks that were most likely caused by thermal stress that built up during the drying process. This is consistent with the literature review [38].

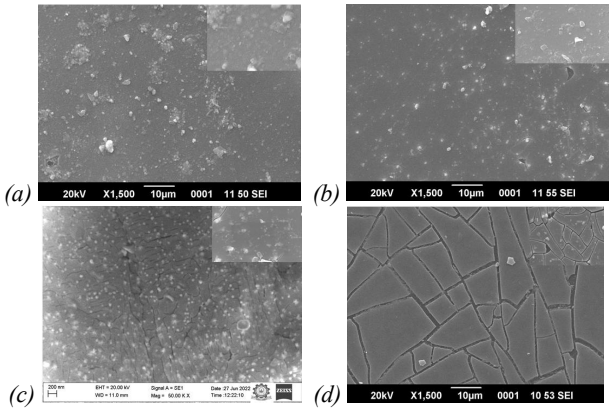

Fig. 1. SEM images of SnO_2 thin films (a) 313 K, (b) 333 K, (c) 353 K, and (d) 373 K

The elemental composition of SnO_2 thin films was determined by EDAX spectrum. Quantitative analysis of the film was investigated by using the EDAX technique for thin films prepared (313, 333, 353 and 373 K) to study the composition in the film as shown in fig. 2. The formation of SnO_2 product confirmed by the presence of Sn and O is observed in the EDAX. The atomic % of Sn and O and their corresponding value are listed in tab. 1 showing that the sample was slightly tin rich, which is in good agreement with the previous reports [39]. The elemental analysis verifies purity of the prepared thin films.

The cassiterite structure from Crystallography Open Database (COD ID 1000062) was used as a starting point for modeling thin films of SnO_2. It belongs to the space group $P4_2/mnm$ with the cell parameters $a = b$ 4.7380 Å, $c = 3.1865$ Å.

The unit cell was propagated to sizes 10×10×534 along the axes *a*, *b* and *c*, so as to achieve the experimentally observed size of 170 nm along the c axis. The constructed nanocluster contains 679 764 atoms in which 228 808 tin atoms and 450 956 oxygen atoms that correspond to the composition $SnO_{1.9709}$ or 33.66 atomic % of tin and 66.34 atomic % of oxygen. However, the experimental composition of thin SnO_2 films, in contrast to cassiterite, contains a much larger amount of tin and a smaller amount of oxygen (e.g. 50.7 atomic % of tin and 48.6 atomic % of oxygen at bath temperatures 313 and 333 K. To achieve such a composition, it is necessary to remove 262 460 oxygen atoms from the structure of the constructed nanocluster. Then, the particle will contain 417 304 atoms with 228 808 tin atoms and 188 496 oxygen atoms that correspond to the composition $SnO_{0.8238}$ or 50.7 atomic % of tin and 48.6 atomic % of

oxygen. Thus, in the process of thin films of SnO_2 preparing, its reduction actually occurs.

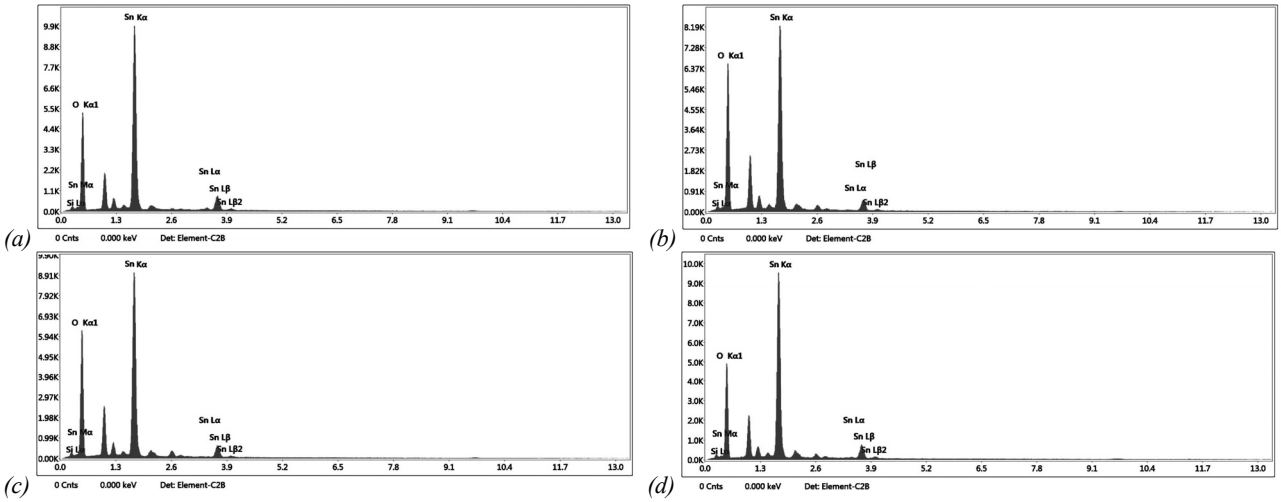

Fig. 2. EDAX spectra of SnO_2 thin films (a) 313 K, (b) 333 K, (c), 353 K, and (d) 373 K

Tab. 1. Atomic percentage of elements at different bath temperatures

Bath temperatures (K)	(Sn (Atomic %), O (Atomic %) and Si (Atomic %))
313 K	50.7, 48.6 and 0.7
333 K	41.4, 58.3 and 0.3
353 K	43.1, 56.4 and 0.5
373 K	48.4, 51.0 and 0.6

For the construction of a particle with such composition, 262 460 oxygen atoms were removed 1 000 000 times from the structure of the initial nanocluster (a variant of the Monte Carlo method) with the consequent estimation of the Gibbs free energy of each 1 000 000 obtained particles at bath temperature 313 K using periodic boundary conditions along a and b axes. The least Gibbs free energy particle was used for further computational study. The usage of periodic boundary conditions along a and b axes within the MERA approach allows us to simulate a quasi-infinite thin SnO_2 film with a thickness of 170 nm, therefore the constructed particle was called the elemental structural component (ESC) of a thin SnO_2 film.

The Gibbs free energy obtained for the ESC accounting periodic boundary conditions is -41.46 kJ per mol of atoms (pma). The calculation per 1 mol of atoms was done because the ESC does not have the stoichiometric composition of SnO_2 and the Gibbs free energy of the entire ESC is divided by the total number of atoms. The enthalpy of the formation is -32.97 kJ·pma and the entropy is 27.14 J pma. The fragment of the ESC is represented in fig. 3.

The elucidation of the ESC structure shows the following. The structure of the ESC retains many symmetry elements of the initial crystal (see fig. 4). As a result of the Monte Carlo procedure, oxygen atoms were removed mainly from the surface of the ESC, moreover, as a rule, from the AOB plane of the initial crystal, which corresponds to the surface of the thin film. The portion of the tin accessible surface is 54.46 % while this one of the oxygen is 45.54 % that approximately agrees with the thin film total composition (tab. 1). More detailed study of the fragments of the surface shows that on the surface of the thin film, the tin chains are formed due to the removal of oxygen so as it is represented in fig. 5*a*. The chains usually include 3 – 5 tin atoms located at a distance of 3.186 – 3.187 Å from each other. These values are slightly greater than two covalent radii of tin (2×1.45 Å = 2.90 Å) and noticeably less than its two van der Waals radii (2×2.17 Å = 4.34 Å) but nevertheless, the observed values are closer to the covalent bond length that provides a conductivity of the thin film. At the same time, in the directions *a* and *b* perpendicular to the *c* axis (fig. 5*b*), an almost strict order of the initial crystal with alternating tin and oxygen atoms is observed.

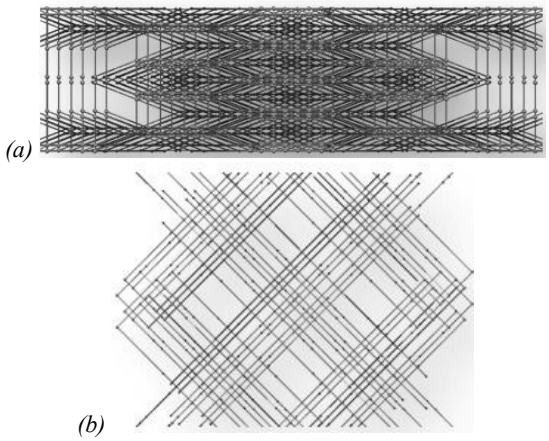

Fig. 3. The structure of the ESC fragment. View along: a) c axis; b) a or b axis

In order to explain the decrease in oxygen content in the SnO_2 thin film (353 K and 373 K), the modeling of oxygen elimination is performed within the MERA approach. The modeled process is as follows

$$ESC \rightarrow ESC(-O_2) + O_2,$$

where $ESC(-O_2)$ is ESC without oxygen.

For modeling of oxygen elimination, as above, an oxygen molecule was removed 1 000 times from the structure of the ESC (a variant of the Monte Carlo method)

with the consequent estimation of the Gibbs free energy of each 1 000 obtained particles using periodic boundary conditions along *a* and *b* axes. The least Gibbs free energy particle was used for further study.

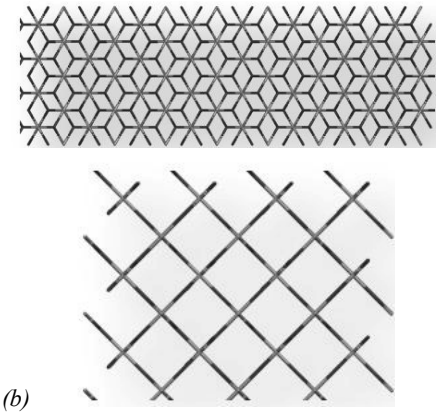

(a)

(b)

Fig. 4. The structure of the initial crystal fragment. View along: a) c axis; b) a or b axis

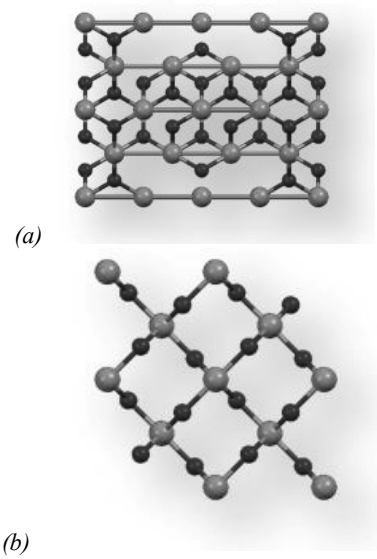

(a)

(b)

Fig. 5. Enlarged fragment of surface. View along: a) c axis; b) a or b axis

The products' enthalpy of the formation is – 28.53 kJ pma and the entropy is 40.22 J pma. Thus, both enthalpy and entropy increase during the process. Both are well explained. The elimination of oxygen requires the breaking of several bonds, which requires energy, and as a result of the process, only one bond O-O is formed. The increase in entropy is well explained by the existence of the gaseous component in products. The calculation of the Gibbs free energy (ΔG) of the process according to the traditional formula

$$\Delta G = \Delta H - T\Delta S \qquad (1)$$

(Where ΔH is the process enthalpy; ΔS is the process entropy) and then the calculation of equilibrium constants (K_e) using van't Hoff equation for 313 K to 373 K temperatures shows the following (tab. 2). For the bath temperatures 313 K and 333 K, the ΔG is positive and K_e is less than zero that indicates thermodynamically unfavorable process of O_2 elimination while for the bath temperatures 353 K and 373 K, the ΔG is negative and K_e are greater than zero that indicates the thermodynamically favorable process of O_2 elimination. It is possible to determine the bath temperature when the elimination process becomes favorable from the equation (1) if we equate ΔG to zero and solve for T. So, the obtained value is $T = 339$ K. Another interesting observation: the ratio of atomic % of Sn and O correlates well with the equilibrium constant (correlation coefficient is 0.945).

Tab. 2. The thermodynamic characteristics and the ratio of atomic % of Sn and O (Ratio) for the process of O_2 elimination at different bath temperatures

Thermodynamic characteristics	Bath temperature (313, 333, 353 and 373 K)
ΔG, kJ pma	0.34, 0.08, – 0.18 and – 0.44
K_e	0.88, 0.97, 1.06 and 1.15
Ratio	1.21, 1.21, 2.54 and 3.62

The modeling of SnO_2 thin films with the composition at 353 K and 373 K performed using the approach described in materials and methods, showed the elongation of tin chains to 5–7 atoms, which should lead to an increase in the conductivity of thin SnO_2 films that really is observed. Moreover, the Gibbs free energy related well both with conductivity and activation energy (E_a). The equations for dependencies shown in fig. 6 look as follows

$$\sigma = 0.2297\cdot 10^{-3} + 0.1793\cdot 10^{-4}\exp(-6.9574\cdot\Delta G) \qquad (2)$$

Correlation coefficient $R = 0.999$

And

$E_a = 0.475 + 0.96\cdot\Delta G$

$R = 0.957$.

The analogous dependencies of σ and E_a on K_e are also observed.

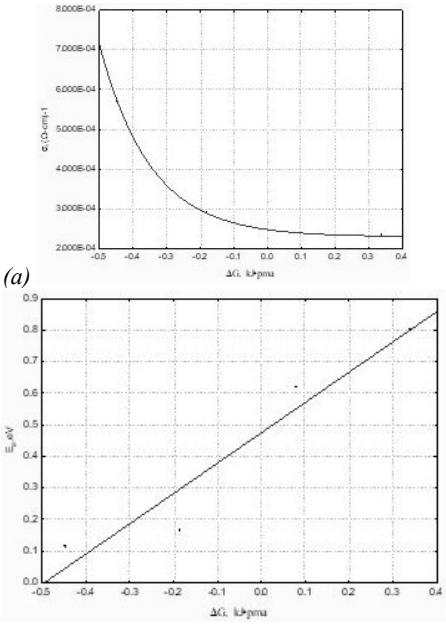

(a)

(b)

Fig. 6. The dependency of a) conductivity and b) E_a on ΔG

Moreover, the existence of metal chains must influence optical properties too. Actually, the band gap (table 3) is dependent both on ΔG and on K_e (fig. 7). The equations for dependencies shown in fig. 7 look as follows

$$\Delta E = 2.724 + 1.26 \cdot \Delta G \quad (3)$$
$$R = 0.977$$
$$\Delta E = 6.31 - 3.59 \cdot K_e$$
$$R = 0.979.$$

Tab. 3. Bandgap energies of the prepared SnO_2 thin films

Different parameters	Bath temperature (313, 333, 353 and 373 K)
Type of transition	Direct allowed, Direct allowed, Direct allowed and Direct allowed
Bandgap energy (eV)	3.21, 2.80, 2.37 and 2.27
lower cutoff wavelength (nm)	392, 372, 320 and 304

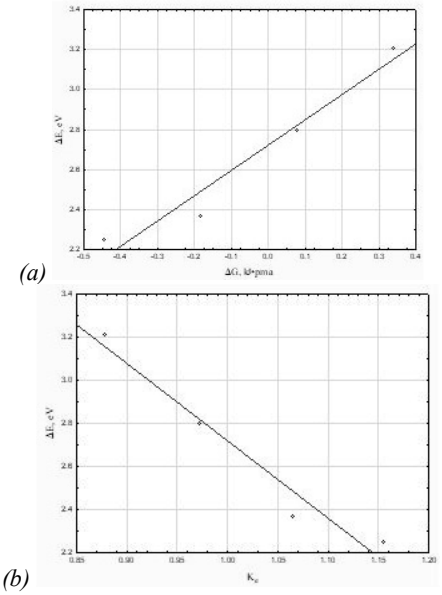

Fig. 7. The dependencies of the band gap energies (ΔE) on a) E_a and b) K_e

UV-Vis spectrum was recorded in the range of 200 – 1100 nm wavelength by three regions; (i) 200 – 400 nm, (ii) 400 – 800 nm, and (iii) 800 – 1100 nm, respectively. The transmittance spectra of SnO_2 thin films prepared (313, 333, 353, and 373 K) are shown in fig. 8*a*. The value of transmittance in the UV region is found to be increased sharply with increasing wavelength and becomes almost constant towards the visible region. In addition, the lower cutoff wavelength was found to be at 304 – 392 nm, and it shows transparency in the visible region. Moreover, the transmittance value is very low and occurred in the range of 300 – 900 nm; on the other hand, it was increasing of the wavelength when the wavelength is longer than 900 nm [40]. The calculated direct bandgap of SnO_2 thin films (fig. 8*b*) in the range of 2.25 – 3.21 eV clearly indicates that tab. 3, which compares well with the reported value of 3.66 eV [41].

In the present study, four probe instruments fixed in the temperature range 303 – 403 K which is used for finding the electrical resistivity of the SnO_2 thin films and it is shown in fig. 9. By utilizing four electrical contacts with the sample surface the electrical measurement is performed. Two of the probes are used to measure the current, while the other two are used to measure the corresponding voltage.

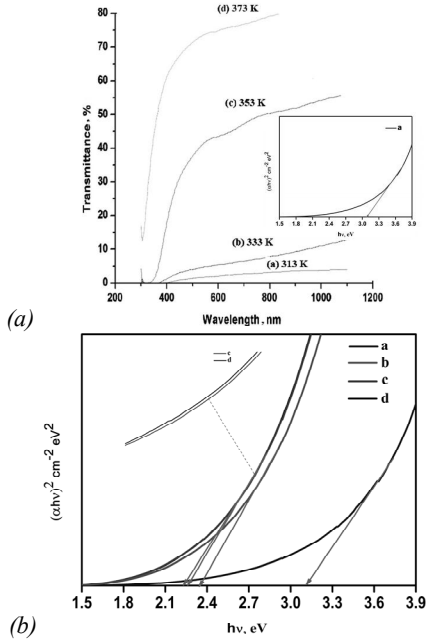

Fig. 8. (a) Optical spectra of SnO_2 thin film prepared (313 K, 333 K, 353 K and 373 K) with inserted Tauc plot (313 K) image.(b) Plot of $(\alpha h\upsilon)^2$ vs. $h\upsilon$ for SnO_2 thin films at different temperatures

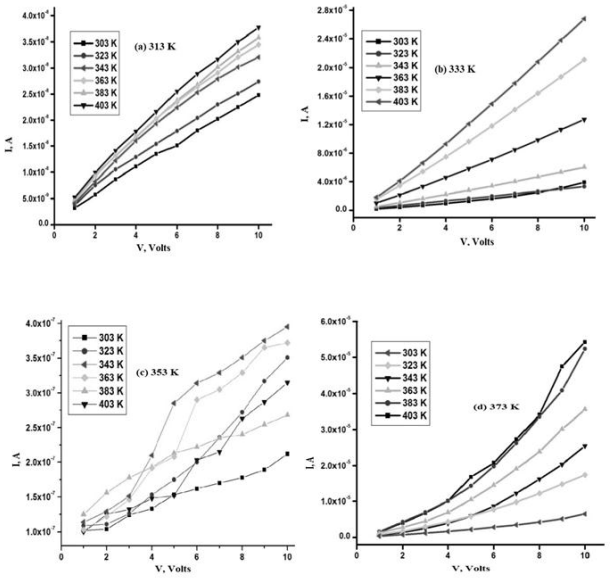

Fig. 9. I–V characteristics of SnO_2 thin film prepared (a) 313 K (b) 333 K (c) 353 K and (d) 373 K

The electrical conductivity of samples are calculted by using the equation,

$$\rho = (\pi / \ln(2)) \cdot (V/I) \cdot t)) \quad (4)$$

Where, I is the current, V is the applied voltage and t is the thickness of the sample, respectively. The rectifying behavior was investigated in the following manner. In that case, we applied voltage (1 to 10V) in steps of 1 V. I was automatically measured with a delay time of 2 sec by concerning each voltage increment. Analyzing current-voltage (I-V) data for all selected temperatures was transmitted to the computer and stored in a computer for additional data analysis. Furthermore, reversing the polarity of contacts several times was carried out for I-V measurements for each sample. The results of the I-V characteristics of samples are shown in fig. 9. From the results, the curves are linear; it may suggest that ohmic conduction by the incidence of thermally generated carriers [42].

The electrical conduction process is limited by thermally activated carriers, and this process continues in the expectation of the injected free carrier density being comparable with the following two examples. (i) Carrier density produced by heat (ii) The conduction current is primarily responsible for injected space charge at sufficiently high fields.

In the current analysis, when the same field is applied, the current rises as the temperature in the ohmic region rises. According to the findings, it can lead to the thermal ionization of trapping centres, a shift in the quasi Fermi stage, and a lowering of the barrier crosswise through which electrons are transported, causing conduction to enter the nearly ohmic region [43].

As noticed in the fig. 10, conductivity (σ) increases with respect to the temperature increasing in the whole range 303 to 403 K by all cases. This is a significant characteristic of semiconducting behavior. At the bath temperature 313 K, the value of DC conductivity of SnO_2 thin film is 0.232×10^{-3} S/cm. Further, the bath temperature increase, the σ values are in 0.232×10^{-3}–0.567×10^{-3} S/cm. SnO_2 thin films conductivity raises gradually by a few orders of magnitude [16].

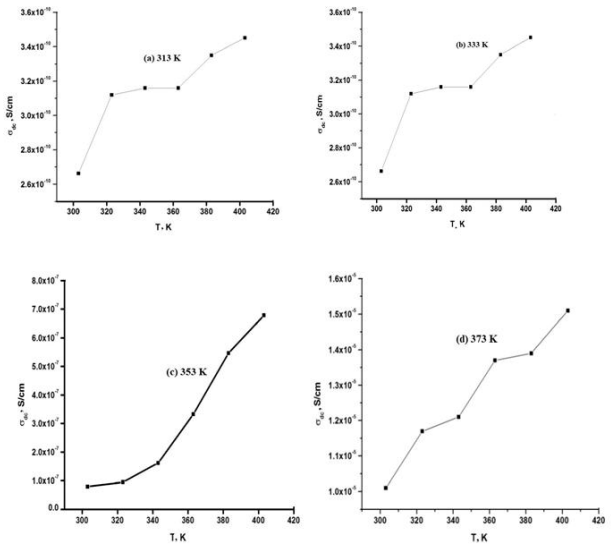

Fig. 10. Temperature Vs Conductivity of SnO_2 thin film prepared (a) 313 K, (b) 333 K, (c) 353 K and (d) 373 K

SnO_2 thin films conductivity increased slightly with respect to the increase of the bath temperature and it may cause by not only be the reason for mobility of charge carriers at the Fermi level. Moreover, it may also due to the occurrence of a higher quantity of conducting species [44 – 46].

$$\rho = \rho_0 \exp\left(E_a / KT\right) \quad (5)$$

At different constant applied voltages, the activation energy (E_a) is calculated using the above equation and by plotting the values of $1000/T$ against $\ln\sigma_{dc}$ as shown in fig. 11. Jonscher and Ansari [45] pointed out ΔE values. According to their theory, a value of less than 0.8 eV indicates that the dominant charge transport occurs due to electron movement. If the value is greater than 0.8 eV, it indicates that ionic charge transport is dominant. In this analysis, ΔE values are associated with Jonscher and Ansari's findings, implying that electronic conduction dominance is important in all samples [45].

Arrhenius plot was used for the calculation of activation energy values of SnO_2 thin films entire temperature range (313 – 373 K). The activation energy values are in the range of 0.80 – 0.11 eV. It clearly confirmed that the bath temperature of the sample increases with the direct relationship of increase in conductivity. The decrease in activation energy with different bath temperatures at 333, 353, and 373 K are noticed. It may suggest that potential barriers are lowered by the presence of an external electric field. Moreover, by using Perlman initial rise method [47] with separating the individual peak from the composite curves, the activation energies for charge transport mechanics were measured. The slopes of plots give the information of activation energies from the initial rising portion of individual peaks and the results are shown in fig. 11.

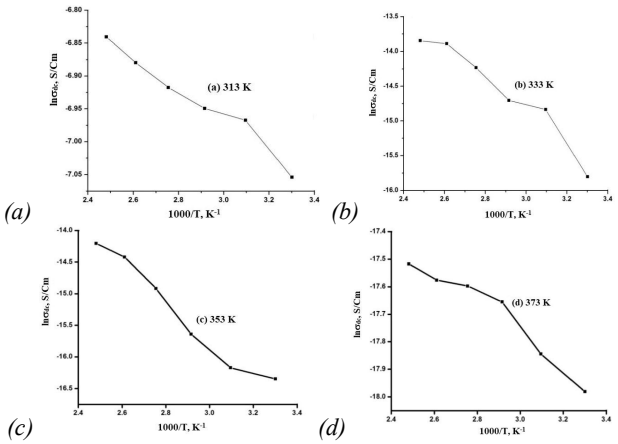

Fig. 11. 1000/T Vs $\ln\sigma_{dc}$ of SnO_2 thin film prepared (a) 313 K, (b) 333 K, (c) 353 K and (d) 373 K

Raman analysis of the prepared samples were performed using Laser Raman spectrometer (Acton SpectraPro 2500i, Princeton Instruments, Acton Optics & Coatings). The major characteristic peaks of SnO_2 thin films prepared (313, 333, 353, and 373 K) is shown in fig. 12. The peak at 2437 cm^{-1} is originating from envi-

ronmental light. The Raman band at 1089 cm^{-1} is attributed to the stretching vibration of SiO bond of SiO_4 tetrahedral unit with one NBO, that is, $[SiO_4]^-$ units in silicate glasses. The Raman active mode E_1g is situated at 475 cm^{-1} for all prepared samples. These Raman results confirms the tetragonal rutile structure of SnO_2 [48, 49]. The doubly degenerate E_1g mode is related to the vibration of oxygen in the oxygen plane. When compared to samples that were annealed at high temperatures, the as-grown sample exhibits comparatively low intensity and broader peaks, which suggests the presence of imperfect lattice sites and an amorphous phase. The annealed samples' increased crystalline SnO_2 grain size is evident from the Raman bands' increased intensity. These findings demonstrate that the crystalline size in the as-grown stage is significantly smaller than in the heat-treated samples.

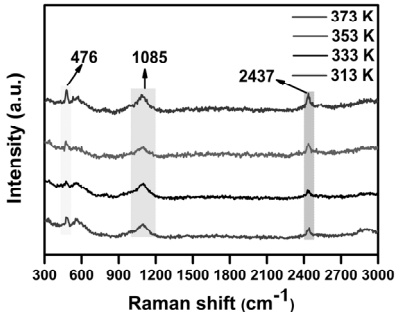

Fig. 12. Raman Spectrum of SnO_2 thin films at different temperatures

Conclusion

In conclusion, the correlation between the computational and experimental studies of tin oxide (SnO_2) thin films prepared by dip-coating technique (313, 333, 353 and 373 K) and annealed at 673 K has reported. SEM results show spherical shape with the agglomeration of the samples. The presence of tin and oxide elements and non-stoichiometric nature were found from the EDAX analysis. Therefore, the SnO_2 thin films microstructures are simulated, their thermodynamic and surface properties are calculated. It was determined that the reason for the change in the composition of SnO_2 thin films with increasing bath temperature is a decrease in the Gibbs free energy due to the entropy factor. The computational study of micromorphology of SnO_2 thin films shows the existence of Sn_n chains ($n = 3-7$, dependently on the bath temperature) on the thin films that cause an increase of conductivity, a decrease in the activation energy of conductivity, and a decrease in band gaps, that actually are experimentally observed. The quantitative models relating these experimental properties with the calculated thermodynamic properties were constructed. Furthermore, Optical characteristics were measured from the transmittance spectra in the UV-VIS region using the envelop method. I-V characteristics results confirmed that the semiconducting nature of the films. From the results, curves are like linear; it may suggest that ohmic conduction due to the occurrence of thermally generated carriers. The estimated electrical conductivity of SnO_2 films is obtained in the range of 0.232×10^{-3} (Ω-cm) to 0.567×10^{-3} (Ω-cm). It is also observed that conductivity of SnO_2 thin films conductivity increases with respect to increase of the bath temperature and it may be caused by two reasons, mobility of the charge carriers at the Fermi level and the presence of a higher quantity of conducting species. The results of electrical conductivity studies confirmed that the highest conductivity (σ) samples acquire the lowest activation energy and their values are in the semiconducting range.

Acknowledgements

The work was supported by Act 211 Government of the Russian Federation, contract 02.A03.21.0011 and by the Ministry of Science and Higher Education of Russia (Grant FENU-2020-0019).

References

[1] Mazur M, Domaradzki J, Wojcieszak D. Optical and electrical properties of (Ti-V)Ox thin film as n-type Transparent Oxide Semiconductor. B Pol Acad Sci-Tech 2014; 62: 583-588. DOI: 10.2478/bpasts-2014-0063.

[2] Karthik K, Pushpa S, Madhukara Naik M, Vinuth M. Influence of Sn and Mn on structural, optical and magnetic properties of spray pyrolysed CdS thin films. Mater Res Innov 2020; 24: 82-86. DOI: 10.1080/14328917.2019.1597436.

[3] Pakiyaraj K, Kirthika V, Karthik K. Effect of annealing on the structural, morphological, optical and electrical properties of Al-Zn co-doped SnO2 thin films. Mater Res Innov 2020; 24: 193-201. DOI: 10.1080/14328917.2019.1628498.

[4] Baden AD, Cox PA, Egdell RG, Orchard AF, Willmer RJD. Observation of surface optical phonons on SrTiO3(100). J Phys C 1981; 14: 1081-1084. DOI: 10.1088/0022-3719/14/34/003.

[5] Diallo A, Manikandan E, Rajendran V, Maaza M. Physical & enhanced photocatalytic properties of green synthesized SnO2 nanoparticles via Aspalathus linearis. J Alloys Compd 2016; 681: 561-570. DOI: 10.1016/j.jallcom.2016.04.200.

[6] Caglar Y, Caglar M, Ilican S, Yakuphanoglu F. Determination of the electronic parameters of nanostructure SnO2/pSi diode. Microelectron Eng 2009; 86: 2072-2077. DOI: 10.1016/j.mee.2009.01.062.

[7] Ravikumar K, Agilan S, Muthukumarasamy N, Raja M, Lakshmanan R, Ganesh R. Influence of annealing temperature on structural and dc electrical properties of SnO2 thin films for schottky barrier diodes. Silicon 2018; 10: 1591-1599. DOI: 10.1007/s12633-017-9643-9.

[8] Dang HP, Luc QH, Le VH, Le T. The influence of deposition temperature and annealing temperature on Ga-doped SnO2 films prepared by direct current magnetron sputtering. J. Alloy. Compd 2016; 687: 1012-1020. DOI: 10.1016/j.jallcom.2016.06.236.

[9] Remes Z, Vanecek M, Yates HM, Evans P, Sheel DW. Optical properties of SnO2:F films deposited by atmospheric pressure CVD. Thin Solid Films 2009; 517: 6287-6289. DOI: 10.1016/j.tsf.2009.02.109.

[10] Choi M-J, Cho CJ, Kim K-C, Pyeon JJ, Park H-H, Kim H-S, Han JH, Kim CG, Chung T-M, Park TJ, Kwon B, Jeong DS, Baek S-H, Kang C-Y, Kim J-S, Kim SK. SnO2 thin films grown by atomic layer deposition using a novel Sn precursor. Appl Surf Sci 2014; 320: 188-194. DOI: 10.1016/j.apsusc.2014.09.054.

[11] Kim GW, Sung CH, Anwar MS, Seo YJ, Heo SN, Park KY, Song TK, Koo BH. Effect of trivalent element doping on structural and optical properties of SnO2 thin films grown by pulsed laser deposition technique. Curr Appl Phys 2012; 12: S21-S24. DOI: 10.1016/j.cap.2012.05.041.

[12] Abdelkrim A, Rahmane S, Abdelouahab O, Abdelmalek N, Brahim G. Effect of solution concentration on the structural, optical and electrical properties of SnO2 thin films prepared by spray pyrolysis. Optik 2016; 127: 2653-2658. DOI: 10.1080/14328917.2019.1628498.

[13] Al-Jawad SMH. Influence of multilayer deposition on characteristics of nanocrystalline SnO2 thin films produce by sol-gel technique. Optik 2017; 146: 17-26. DOI: 10.1016/j.ijleo.2017.08.053.

[14] Carvalho DHQ, Schiavon MA, Raposo MT, de Paiva R, Alves JLA, Paniago RM, Speziali NL, Ferlauto AS, Ardisson JD. Synthesis and characterization of SnO2 thin films prepared by dip-coating method. Physics Procedia 2012; 28: 22-27. DOI: 10.1016/j.phpro.2012.03.664.

[15] Gurushankar K, Gohulkumar M, Viswanathan K, Revathy MS, Jeyavijayan S. Structural analysis of SnO2 thin films at various temperatures (313, 333, 353 and 373 K). International Journal of Recent Technology and Engineering 2019; 8: 914-916.

[16] Sivasenthil E, Senthilkumar V. Electrical characterization of tin oxide thin films prepared by dip coating technique. Int J Innov Res Technol Sci Eng 2016; 5: 14651-14655.

[17] Acciarri M, Canevali C, Mari CM, Mattoni M, Ruffo R, Scotti R, Morazzoni F, Barreca D, Armelao L, Tondello E, Bontempi E, Depero LE. Nanocrystalline SnO2-based thin films obtained by sol-gel route: A morphological and structural investigation. Chem Mater 2003; 15: 2646-2650. DOI: 10.1021/cm031002w.

[18] Manakov AY, Likhacheva AY, Potemkin VA, Ogienko AG, Kurnosov AV, Ancharov AI. Compressibility of gas hydrates. ChemPhysChem 2011; 12: 2476-2484. DOI: 10.1002/cphc.201100126.

[19] Aladko EY, Ancharov AI, Goryainov SV, Kurnosov AV, Larionov EG, Likhacheva AY, Manakov AY, Potemkin VA, Sheromov MA, Teplykh AE, Voronin VI, Zhurko FV. New type of phase transformation in gas hydrate forming system at high pressures. Some experimental and computational investigations of clathrate hydrates formed in the SF6-H2O system. J Phys Chem B 2006; 110: 21371-21376. DOI: 10.1021/jp061698r.

[20] Sukharev YI, Potemkin VA, Markov BA. Autowave processes of forming gels as a cause of the coloring of oxyhydrate gels (the chromatic effect) of some rare earth metals (yttrium, gadolinium). Colloids Surf A 2001; 194: 75-84. DOI: 10.1016/S0927-7757(01)00757-9.

[21] Potemkin VA, Maksakov VA, Kirin VP. Conformational States of triosmium clusters with aminoacid ligands: A theoretical study. J Struct. Chem 2003; 44: 741-747. DOI: 10.1023/B:JORY.0000029809.88411.8b.

[22] Korenev VS. Kirin VP, Maksakov VA, Virovets AV, Tkachev SV, Potemkin VA, Agafontsev AM, Tkachev AV. Triosmium cluster with the bridging aminooxime derivative of pinane: synthesis, crystal structure and conformational analysis. Russ J Coord Chem 2007; 33: 594-600. DOI: 10.1134/S1070328407080088.

[23] Bannikov VV, Shein IR, Kozhevnikov VL, Ivanovskii AL. Electronic structure and magnetic properties of double perovskites Sr2FeMO6 (M = Sc, Ti,...,Ni, Cu) according to the data of FLAPW-GGA band structure calculations. J Struct Chem 2008; 49: 781-787. DOI: 10.1007/s10947-008-0139-8.

[24] Maksakov VA, Pervukhina NV, Podberezskaya NV, Afonin MY, Potemkin VA, Kirin VP. X-ray and conformation analysis of the new trinuclear cluster of osmium Os3 (μ, η2-OCC6H5) (η3-C3H5) (CO)9. J Struct Chem 2008; 49: 894-900. DOI: 10.1007/s10947-008-0154-9.

[25] Kuzmicheva GA, Jayanna PK, Eroshkin AM, Grishina M A, Pereyaslavskaya ES, Potemkin VA, Petrenko VA. Mutations in fd phage major coat protein modulate affinity of the displayed peptide. Protein Eng Des Sel 2009; 22: 631-639. DOI: 10.1093/protein/gzp043.

[26] Potemkin VA, Ivshina NN, Maksakov VA. Theoretical study of the conformational features of triosmium clusters. J Struct Chem 2009; 50: 143-151. DOI: 10.1007/s10947-009-0202-0.

[27] Ivshina NN, Bartashevich EV, Potemkin VA, Grishina MA, Ishmetova RI, Rusinov GL, Latosh NI, Slepukhin P, Charushin VN. Changes in the vibrational characteristics of substituted 1,2,4,5-tetrazines after complexation with 1,2,3- benzotriazole: A theoretical study. J Struct Chem 2010; 50: 1053-1058. DOI: 10.1007/s10947-009-0155-3.

[28] Potemkin VA, Krasnov VP, Levit GL, Bartashevich EV, Andreeva IN, Kuzminsky MB, Anikin NA, Charushin V N, Chupakhin ON. Kinetic resolution of (±)-2,3-dihydro-3-methyl-4H-1,4-benzoxazine in the reaction with (S)-naproxen chloride: a theoretical study. Mendeleev Commun 2004; 14: 69-70. DOI: 10.1070/MC2004v014n02ABEH001887.

[29] ChemoSophia. Source: ⟨http://www.chemosophia.com/⟩.

[30] Potemkin VA, Maksakov VA, Korenev VS. Theoretical study of the conformational states of triosmium clusters with a chiral pinane ligand. J Struct Chem 2005; 46: 43-48. DOI: 10.1007/s10947-006-0007-3.

[31] Sukharev YI, Avdin VV, Lymar AA, Belkanova MY, Potemkin VA. Directions in structure formation of oxyhydrate gels of zirconium and rare earth elements. J Struct Chem 2006; 47: 151-155. DOI: 10.1007/s10947-006-0280-1.

[32] Potemkin VA, Maksakov VA, Korenev VS. Theoretical study of the conformational states of triosmium clusters with a chiral μ-1-NH pinane ligand. J Struct Chem 2007; 48: 225-230. DOI: 10.1007/s10947-007-0036-6.

[33] Avdin VV, Lymar AA, Batist AV, Nikitin EA, Belkanova MY, Potemkin VA, Structure formation in heavy metal oxyhydrates at low rates of gel formation. J Struct Chem 2007; 48: 747-752. DOI: 10.1007/s10947-007-0114-9.

[34] Shchelokov A, Palko N, Potemkin V, Grishina M, Morozov R, Korina E, Uchaev D, Krivtsov I, Bol'shakov O. Adsorption of native amino acids on nanocrystalline TiO2: physical chemistry, QSPR, and theoretical modeling. Langmuir 2019; 35: 538-550. DOI: 10.1021/acs.langmuir.8b02007.

[35] Moman E, Grishina MA, Potemkin VA. Nonparametric chemical descriptors for the calculation of ligand-biopolymer affinities with machine-learning scoring functions. J Comp-Aid Mol Des 2019; 33: 943-953. DOI: 10.1007/s10822-019-00248-2.

[36] Korina E, Naifert S, Morozov R, Potemkin V, Bol'shakov O. Study of short peptide adsorption on solution dispersed inorganic nanoparticles using depletion method. JoVE 2020; 158: e60526. DOI: 10.3791/60526.

[37] Matei ghimbeu C, Van landschoot RC, Schoonman J. Preparation and characterization of SnO2 and Cu-doped SnO2 thin films using electrostatic spray deposition (ESD). J Eur Cer Soc 2007; 2: 207-213. DOI: 10.1016/j.jeurceramsoc.2006.05.092.

[38] Bockmeyer M, Löbmann P. Crack formation in TiO_2 films prepared by sol–gel processing: Quantification and characterization. Thin Solid Films 2007; 515: 5215-5219. DOI: 10.1016/j.tsf.2006.11.193.

[39] John VS, Mahalingam T, Chu JP. Synthesis and characterization of copper doped zinc telluride thin films. Solid State Electronics 2005; 49: 3-7. DOI: 10.1016/j.sse.2004.07.015.
[40] Abdelaziz M, Ghannam MM. Influence of titanium chloride addition on the optical and dielectric properties of PVA films. Physica B 2010; 405: 958-964. DOI: 10.1016/j.physb.2009.10.030.
[41] Majumder S. Synthesis and characterisation of SnO2 films obtained by a wet chemical process. Materials Science-Poland 2009; 27: 123-129.
[42] Verma A, Khare PK, Srivastava RK. Electrode effect on electrical conduction in thin film of polyvinyl pyrrolidone. Indian J Pure Appl Phys 2009; 47: 737-744.
[43] Ramu C, Naidu YRV, Sharma AK. Dielectric relaxation in iodine doped cellulose acetate films. Ferroelectrics 1994; 159: 275-280. DOI: 10.1080/00150199408007585.
[44] Abd-El Kader FH, Osman WH, Hafez RS. DC conduction mechanism and dielectric properties of Poly (methyl methacrylate)/Poly (vinyl acetate) blends doped and undoped with malachite green. Physica B 2013; 408: 140-150. DOI: 10.1016/j.physb.2012.09.027.
[45] Jonscher AK, Ansari AA. Photo-currents in silicon monoxide films. Phil Mag 1971; 23: 205-223. DOI: 10.1080/14786437108216374.
[46] Perlam MM. Thermal currents and the internal polarization in carnauba wax electrets. J Appl Pys 1971; 42: 2645.
[47] Tiwari A, Singh S. Synthesis and characterization of electrical conducting chitosan-graft-polyaniline. Exp Polym Lett 2007; 1: 308-317. DOI: 10.3144/expresspolymlett.2007.44.
[48] Xi L, Qian D, Tang X, Chen C. High surface area SnO2 nanoparticles: synthesis and gas sensing properties. Mater Chem Phys 2008; 108: 232-236. DOI: 10.1016/j.matchemphys.2007.09.023.
[49] Sangeetha P, Sasirekha V, Ramakrishnana V. Micro-Raman investigation of tin dioxide nanostructured material based on annealing effect. J Raman Spectrosc 2011; 42: 1634-1639. DOI: 10.1002/jrs.2919.

Authors' information

K. Gurushankar, (b. 1987) done his Ph.D at Annamalai University, Tamilnadu in 2015, majoring in Ph.D. Currently he works as the Senior Researcher, Laboratory of Computational Modeling of Drugs, South Ural State University, Chelyabinsk, Russia. He has published more than 30 research articles in reputed journals including Thomson Reuters (SCI & Web of Science) and conferences and it's also available online. He has total citations: 361, h-index: 11, i-10 index: 12. Research interests are molecular modeling of phytopreparations, nanotechnology and DFT study for drug design. E-mail: *gurushankar01051987@gmail.com* .

M. Grishina, (b. 1977), works as a Principal Scientist, Laboratory of Computational Modeling of Drugs, South Ural State University, Chelyabinsk, Russia. Research interests: molecular modeling and theoretical drug design.
E-mail: *grishinama@susu.ru* .

M. Gohulkumar, (b. 1986), done his Ph.D at Annamalai University, Tamil Nadu in 2015, majoring in Ph.D. Currently he works as the Assistant Professor, Physics Department, Vivekananda College of Arts and Science for Women, Tiruchengode, Tamil Nadu, India. Research interests are nanotechnology and applied spectroscopy.
E-mail: *ghoul_phy@yahoo.co.in* .

Karthik Kannan, (b. 1989), done his Ph.D at Bharathidasan University, Tamil Nadu in 2019, majoring in Ph.D. Currently working as Brain Fool Fellow, School of Advanced Materials Science and Engineering, Kumoh National Institute of Technology, Republic of Korea. He has published more than 100 research articles in reputed journals including Thomson Reuters (SCI & Web of Science) and conferences and it's also available online. He has total citations: 2850, h-index: 33, i-10 index: 63. His current research interests are 2D nanomaterials for hydrogen generation, carbon dioxide conversion, fuel cells, environmental, and biological applications.
E-mail: *karthikkannanphotochem@gmail.com* .

Received April 22, 2022. The final version – September 22, 2022.